An improved Graph-based SNR Estimation Algorithm

Li Yang[1], Haoyu Wei[1], Guobing Hu[1]*, Wenqing Zhu[2]
[1] School of Electronic and Information Engineering, Jinling Institute of Technology, Nanjing, Jiangsu Province 211169, China
[2] School of Information Science and Technology, Artificial Intelligence, Nanjing Forestry University, Nanjing, Jiangsu Province 210037, China
[e-mail: yangli691@163.com, 2460040789@qq.com, njcithgb@163.com, 1458561045@qq.com]
*Corresponding author: Guobing Hu

Received September 4, 2023; revised July 30, 2024; revised September 5, 2024; accepted October 9, 2024; published October 31, 2024

Abstract

The previous graph-based estimation algorithm is of poor performance in low signal-to-noise ratio (SNR) and is failure for frequency band signals. An improved graph-based SNR estimator using blocking sum of spectrum of the observed signal is proposed in this article, which consists of two stages: fitting the SNR estimation expression by training samples and estimating the SNR of the test signal. In the former stage, the training samples are firstly segmented with overlap, then the real part of the spectrum of each segment is blocked without overlap and summed to be transformed to a graph, and accordingly the average degree sum (DS) of the graphs is calculated. Afterwards, a nonlinear fitting of the relationship between the average DS and the SNR is obtained using a trust region fitting algorithm. In the latter stage, the average DS of the test signal is obtained by applying the mentioned scheme. Subsequently, substitute it into the fitted expression to estimate the SNR. Moreover, we analyze the impact mechanism of the order preserving between the majorization order of input samples and the majorization order of vertex probability vectors, which providing a basis for the interpretability of graph-based SNR estimator and for the selection of input forms for graph transform in the estimation. Simulation results demonstrate that the proposed algorithm has a superiority performance for both baseband and frequency band signals under low SNR and multipath or fading channels, with a computational complexity of approximately 50% compared to the existing graph-based algorithm.

Keywords: SNR estimation, Signal to graph convertor, Majorization order, Order-preserving, Normalized root mean square error, Deflection coefficient

1. Introduction

Signal-to-noise ratio (SNR) is a key parameter used to measure the relative strength relationship between a signal and noise [1]. In wireless communication signal processing and radar signal processing aspects, the SNR estimation has wide applications in communication system performance evaluation [2], channel estimation [3], signal detection and demodulation [4], radar target detection and tracking [5], and so on. Generally, SNR estimation algorithm can be broadly categorized into two types: model-driven-based and data-driven-based. Model-driven-based algorithm mainly utilizes the statistical characteristics of signals, such as maximum likelihood estimation [6], higher-order cumulant-based [7], and eigen-decomposition of matrix methods [8]. However, these methods only utilize the statistical characteristics of the signal and do not further explore the correlation information between samples, namely the topological characteristics [9], which limits their estimation performance in a certain sense. With the widespread application of artificial intelligence and neural networks in wireless communication signal processing, data-driven-based have also been widely used, especially deep learning frameworks [10], which is showing promising estimation performance. However, it is evident that these algorithms require a large number of labeled samples and are prone to problems such as overfitting during training. In general, to investigate a novel SNR estimation framework using new features, such as graphical features, and less training samples is a crucial issue. Characteristics and comparison of various existing SNR estimation algorithms are listed in **Table 1** as below.

Table 1. Characteristics and comparison of various existing SNR estimation algorithms

Paper	Main idea	Advantages	Disadvantages
[6]	**ML-based method**: A maximum likelihood SNR estimator for coded linearly modulated signals is proposed. The estimator is expressed in terms of the marginal a posterior probabilities of the coded symbols.	It performs well in low SNR regime by exploiting channel coding characteristics, and its performance is very close to the Cramer-Rao bound.	It requires prior signal information and the computational complexity is high.
[7]	**M2M4-based method**: The SNR estimate is calculated by computing the second and fourth-order moments of the received signal based on its average time.	It is no need to know the modulation method of the transmitted signal, and the receiver does not need to recover the phase information.	The estimation performance worsens as the SNR value increases.
[8]	**SVD-based method**: Singular value decomposition technology is utilized to process the matrix construction called covariance, or Hankel matrix of the signal to estimate the dimensions of the signal and noise subspaces, thereby calculating the SNR.	It does not require prior information, and is suitable for blind signal processing.	When the dimension of the matrix is large, the computational complexity is high.
[11]	**Graph sparsity-based method**: A blind SNR estimation method based on graph sparsity is proposed. By converting the original signal into a graph, the SNR is estimated using the sparsity of the final graph.	It is robustness to multipath channel, noise distributions, and small sample size.	It is not suitable for frequency band signals.

Recently, graph signal processing methods have achieved encouraging results in signal detection [12, 13], modulation recognition [14-16], and credibility evaluation of blind processing results [17]. Generally speaking, this method transforms time series into graphs composed of vertices and edges through normalization, quantization, and graph mapping, fully exploring the potential structural information of the signal. Nevertheless, the application of graph transformation in parameter estimation is still rare, because the quantization process in graph transformation improves the algorithm's resistance to interference, but sacrifices the information of the signal at small scales. In [11], graph signal processing method is applied to SNR estimation of communication signals for the first time. In this article, the algorithm is mainly based on graph transformation of time-domain signals and can be divided into two stages. In the first stage, the real part of the time-domain signal is segmented with overlapping, then the graph transformation is performed segment by segment to obtain the mean value of the sum of adjacency matrixes of each graph, which is defined as the graph sparsity (GS). As a result, an expression for SNR estimation based on the functional mapping from GS to SNR is fitted. In the second stage, for a given test signal, the GS is calculated using the above method, and is substituted into the SNR estimation expression to estimate the SNR. This article provides a new approach for graph-based parameter estimation, whereas it still has the following problems: 1) Even though a functional mapping from GS to the SNR is established, it does not further discuss the inherent mechanism of the mapping from the graph domain to the parameter domain. The necessary conditions for holding this mapping, and the criterion to choose the input to graph transform to obtain more favorable performance to establish this functional mapping have not been rigorously analyzed either theoretically or experimentally. 2) The graph-based SNR estimation problem of the baseband signal is discussed, but its effectiveness for the frequency band signals is not verified. As we know, in practical signal processing, parameter estimation of frequency band signal that has not been demodulated may be more important. By simulations, we further found that for frequency band signals, there is a non-monotonic mapping from the GS to the SNR, which leads to ambiguous performance of the graph-based SNR estimator. 3) The computational complexity is relatively high, which is approximately proportional to $\mathrm{O}(ml + ml^2)$, where m represents the number of segments, and l represents the length of each segmented samples.

To solve the above mentioned questions, we propose a graph-based SNR estimation algorithm based on blocking sum of spectrum (SBS). The basic idea is as follows: In the initial stage, the training signal is segmented with overlapping. For each segment, the real parts of the spectrum of the signals are calculated, and then the SBS of them are transformed into graphs to obtain the the degree sum (DS). Once the DS is obtained for each graph, the average DS is computed. Using the average DS, an expression for SNR estimation is fitted by several training signals. In the second stage, the test signal undergoes the same steps as described above to calculate the average DS, and this value is then substituted into the obtained SNR estimation expression to estimate the SNR of the test signal. Overall, the SBS can reduce the computational complexity of the algorithm by means of decreasing the number of input samples for graph transform. Simulation experiments demonstrate that the proposed algorithm performs well in low SNRs and multipath or fading channels for both bandpass signals and frequency band signals, and the computational complexity is approximately 50% of the existing graph domain algorithm.

The main contributions of this paper are as follows:

1) Considering the graph transformation of the constant plus Gaussian white noise model as an example, we analyze the relationships between the majorization order of vertex probability vectors (VPVs), and the DS of graph under different noise variance. Then, the sufficient

condition for the preserving of the majorization order of VPVs is provided.

2) The ratio of the number of order-preserving for the majorization order of VPVs to the total number of simulations is defined as the order-preserving rate (OPR). Afterwards, the relationships among OPR, the DS and deflection coefficients are investigated, which provide a basis for the selection of the form of the input signals of the graph transformation in SNR estimation in the graph-domain.

3) A graph-based SNR estimation method based on SBS is proposed, and the performance is evaluated under different operating conditions and signal parameters to verify its effectiveness. Meanwhile, the proposed algorithm is compared with the existing graph-based SNR estimation algorithm, the traditional M2M4-based method and SVD-based method in terms of estimation performance and computational complexity to verify its superiority.

This paper is organized as follows. Section II introduces the signal model, the related background of graph-domain signal processing and the definition of several important terms involved in the article. Section III analyzes the limitations of the existing graph-based SNR algorithm, derives the proposed algorithm, and analyzes its computational complexity. The simulation performance analysis and comparisons with other algorithms are provided in Section IV. Section V concludes this article.

2. Signal model and background

2.1 Signal model

Assuming the observed signal is a frequency band signal with additive Gaussian white noise (AGWN), it can be expressed as:

$$x(n) = s(n) \times c(n) + w(n) = A\exp(j[2\pi f_0 n\Delta t + \pi d(n) + \theta]) \times c(n) + w(n), 0 \le n \le N-1 \quad (1)$$

where $x(n)$ is the observed signal, $s(n)$ is the frequency band signal, A is the signal amplitude, N is the length of the signal samples, f_0 is the signal carrier frequency, Δt is the sampling interval, θ is the initial phase of the signal, and $d(n)$ is the phase encoding function, $w(n)$ is the zero-mean AGWN with independent real and imaginary parts, and the variance $2\sigma_0^2$, and $c(n)$ denotes the channel gain defined by:

$$c(n) = \sum_{\ell=1}^{D} h_\ell \delta(n - \kappa_\ell), \quad (2)$$

where D is the channel order, h_ℓ is the gain of the ℓth channel, and κ_ℓ is the delay of the ℓth channel. When a single channel with no attenuation and no delay is considered, the expression for the SNR is given by [11]:

$$\Gamma = \frac{\mathrm{P}(|s(n)|^2)}{\mathrm{P}(|w(n)|^2)}, \quad (3)$$

where $\mathrm{P}(|s(n)|^2)$ is the average power of the signal, $\mathrm{P}(|w(n)|^2)$ is the average power of the noise, and the logarithm form of SNR is computed by $\beta[\mathrm{dB}] = 10\log_{10}\Gamma$.

2.2 Graph transformation

According to [12], let the signal denote as $X(k)$ with length L, the corresponding graph structure can be obtained through the following three steps for a given signal.

1) Normalization: find the maximum and minimum values of $X(k)$, and map all samples to

the interval [0,1] using the following equation:

$$Y(k)=\frac{X(k)-\omega_{\min}}{\omega_{\max}-\omega_{\min}},1\le k\le L, \tag{4}$$

where $Y(k)$ is the normalized sequence, $\omega_{\max}$ and $\omega_{\min}$ are the maximum and minimum values of $X(k)$, respectively.

2) Quantization: set the quantization levels as N_0, and quantize $Y(k)$ with equal intervals:

$$U(k)=z+1,\frac{z}{N_0}<Y(k)<\frac{z+1}{N_0},0\le z\le N_0-1, \tag{5}$$

where $U(k)$ is the quantized sequence, N_0 is the number of quantization levels.

3) Graph mapping: map $U(k)$ to a simple graph $G=(E,V)$, where $E=\{e_{i,j}\mid v_i\in V,v_j\in V\}$ and $V=\{v_1,v_2,...,v_{N_0}\}$ represent the edge and vertex sets of the graph G, respectively. The map scheme is as follows: By Iterating from $U(k)$ to $U(k+1)$, and checking whether there is a level transition from v_i to v_j, if there is a connection between the two vertices, then $e_{i,j}=1$; otherwise, $e_{i,j}=0$.

2.3 Several important definitions

Definition 1 Vertex probability vector (VPV) [18]. Let $\mathbf{p}=(p_1,p_2,...,p_{N_0})^T$, $\mathbf{q}=(q_1,q_2,...,q_{N_0})^T$ be VPV on $G_{\mathbf{p}}$ and $G_{\mathbf{q}}$, respectively, and can be expressed by

$$p_i=I_i(G_{\mathbf{p}})/L,i=1,2...,N_0, \tag{6}$$

$$q_i=I_i(G_{\mathbf{q}})/L,i=1,2...,N_0, \tag{7}$$

where $I_i(G_{\mathbf{p}})$ is the number of edges of the ith vertex of Graph $G_{\mathbf{p}}$, $I_i(G_{\mathbf{q}})$ is the number of edges of the ith vertex of Graph $G_{\mathbf{q}}$.

According to [13, 17], for two independent and identically distributed (I.I.D.) random sequences being transformed to the graphs, their VPVs directly affect the connectivity of the corresponding generated graphs. The more uniform the distribution of the VPV, the stronger the connectivity of the generated graph. Hence, when the number of samples and the number of quantization levels are fixed, the strength of the connectivity of the two graphs can be compared by examining the uniformity of the corresponding VPV.

Definition 2 Majorization order between two different VPVs.

$$S_{\mathrm{p}_\Omega}=\sum_{i=1}^{\Omega}p_{[i]},1\le i,j\le\Omega\le N_0 \tag{8}$$

and

$$S_{\mathrm{q}_\Omega}=\sum_{j=1}^{\Omega}q_{[j]},1\le i,j\le\Omega\le N_0 \tag{9}$$

are the partial sums of VPVs, i.e., $\mathbf{p}$ and $\mathbf{q}$, where $p_{[i]}$ and $q_{[j]}$ is the element of the non-increasing rearrangement. If $S_{\mathrm{p}_\Omega}<S_{\mathrm{q}_\Omega}$, then $\mathbf{p}\prec\mathbf{q}$ holds, which is referred to as $\mathbf{p}$ is majorized by $\mathbf{q}$, indicating that the uniformity of $\mathbf{p}$ is greater than $\mathbf{q}$.

Definition 3 Majorization order of the continuous random variables [19]. Let X_1, X_2 be the continuous random variables with probability density functions (PDF) denoted as $f(x)$ and $g(x)$. For any value of $t>0$, it holds that

$$\int_0^t g^*(x)dx \le \int_0^t f^*(x)dx . \tag{10}$$

In this case, we say that $g(x)$ is majorized by $f(x)$, denoted as $g \prec f$. In (10), $f^*(x)$, $g^*(x)$ are the non-increasing rearrangement functions of $f(x)$ and $g(x)$, respectively, i.e., $f^*(x) = \sup_{\mu(b)>x} b, x \ge 0$ and $\mu(b) = \mu\{x : f(x) > b\}$, where μ is the Lebesgue measure and sup(b) denotes the supremum of b.

Example: If two random variables are both Gaussian distributed continuous random variables, their majorization order is described as follows. Assuming W_1 and W_2 be I.I.D zero-mean Gaussian random variables, i.e., $W_1 \sim N(0,\sigma_1^2)$ and $W_2 \sim N(0,\sigma_2^2)$, ${\sigma_1}^2 > {\sigma_2}^2$, and accordingly, their PDFs are $f_{W_1}(x)$ 和 $f_{W_2}(x)$,then it follows:

$$f_{W_1}(x) \prec f_{W_2}(x), \tag{11}$$

which means $f_{W_1}(x)$ is majorized by $f_{W_2}(x)$, i.e., the distribution of W_1 is more uniform than W_2. It can be deduced that when the time continuous random variables both follow Gaussian distributions, the majorization order can be uniquely determined by their variances. Therefore, the variance can be considered as the uncertainty parameter of Gaussian random variables [19].

Remarks: 1) It should be noted that the VPV is fundamentally the area sampling of the normalized PDF of a random variable [20], which is approximately the same as the PDF of quantized samples. Therefore, the majorization order of VPVs is essentially determined by the majorization order of the original continuous random variables. 2) For the convenience of expression in the successive parts of the article, the majorization order of input sample distribution will be referred to as the input majorization order, the majorization order of normalized sample distribution will be referred to as the normalization majorization order, and the majorization order of VPV will be referred to as quantization majorization order. It is worth noting that, due to the random nature of maximum and minimum of the random samples utilized in (4), the input majorization order and normalization majorization order may not be the same, i.e., non order-preserving. If the quantization majorization order and normalization majorization order are the same, we call it “order-preserving”.

3. Algorithm principle

3.1 Limitations of the existing graph-based SNR estimation algorithm

As mentioned in [11], the accurate estimation of the SNR can be realized by constructing the GS structure using a small sample size. Meanwhile, it is stated in the paper that the GS represents the strength of the connectivity of the graph and also reflects the correlation between the input samples of the graph. However, there are the following problems:

1) The instinct mechanism of the correspondence between the GS and the SNR is not clarified in detail, i.e., the reason that the smaller SNR is corresponding to the larger GS, whereas the larger SNR is corresponding to the smaller GS.

2) Without providing the method to improve the robustness of the mapping relationship between GS and SNR through appropriate preprocessing and the criterion to select the more effective input form fed to graph transformation.

3.2 Majorization orders involved in different input samples

Intuitively, the factors affecting the graph-based SNR estimation performance can be

considered from two aspects: the input samples for graph transformation and the connectivity of the generated graph.

From the perspective of input of graph transformation, the uniformity of the input sample distribution is an important factor affecting the connectivity of the generated graph. Clearly, the input samples need to be normalized and quantized before being transformed into graph. According to [17], the connectivity of the graph is primarily determined by the uniformity of its VPV. Normalization is a linear transformation applied to the original input samples, but the slope of the linear transformation is a random variable, and the uniformity of its distribution may change randomly. On the other hand, quantization does not change the uniformity of the normalized sample distribution. Therefore, order-preserving between the input majorization order and the quantization majorization order should be evaluated. Order-preserving implies that there is a consistent relationship between the uniformity of the input samples and the connectivity of the corresponding generated graphs. In other words, increasing the uniformity of the input samples results in increase of connectivity of the generated graph. Hence, it is desirable to obtain order-preserving or high OPR between the input majorization order, the normalized majorization order and the quantized majorization order. This ensures a consistent relationship between the uniformity of the input samples for graph transformation and the connectivity of the generated graphs, hence improving the performance of the SNR estimation using graphs.

Theorem 1 (Sufficient Condition for order-preserving of majorization order). Let us suppose two continuous random variables of I.I.D. Gaussian distribution, i.e., $X_1 = R + W_1$ and $X_2 = R + W_2$, with their PDF denoted by $f_{X_1}(x)$ and $f_{X_2}(x)$, where R is a real constant. Their SNRs can be obtained by $\gamma_1 = R^2/\sigma_1^2$ and $\gamma_2 = R^2/\sigma_2^2$, respectively. If we normalize X_1 and X_2, as X_1^N and X_2^N, respectively, i.e., $X_1^N = c_1^{-1}X_1 - e_1$, $X_2^N = c_2^{-1}X_2 - e_2$, and their corresponding VPVs are denoted as $\mathbf{p}$ and $\mathbf{q}$, where $c_i = \omega_{\max} - \omega_{\min}$, $e_i = \dfrac{\omega_{\min}}{\omega_{\max} - \omega_{\min}}$. If $\sigma_1^2 > \sigma_2^2$, and $c_1 d_1 < c_2 d_2$, it follows $f_{X_1}(x) \prec f_{X_2}(x)$, and $\mathbf{p} \prec \mathbf{q}$, where $d_i = f_{X_i}^*(0), i = 1, 2$ and $f_{X_i}^*(0)$ denotes the value of non-increasing arrangement of $f_{X_i}(x)$ when $x = 0$.

Proof. According to [19, 21], because $X_1 \sim N\left(R, \sigma_1^2\right)$ and $X_2 \sim N\left(R, \sigma_2^2\right)$, when $\sigma_1^2 > \sigma_2^2$, it follows $f_{X_1}(x) \prec f_{X_2}(x)$. Furthermore, according to [17], when $c_1 d_1 < c_2 d_2$, it follows $\mathbf{p} \prec \mathbf{q}$.

Remarks: Theorem 1 states that when the input samples of graph transformation are the constants with AGWN with different variances, if $c_1 d_1 < c_2 d_2$, the order-preserving occurs between the quantization majorization order and the input majorization order. However, $c_1 d_1 < c_2 d_2$ is only a sufficient condition for order-preserving, not a necessary condition. In other words, even if $c_1 d_1 < c_2 d_2$ is not satisfied, order-preserving can still be possible. But if the order preserving does not hold, the inequality $c_1 d_1 \geq c_2 d_2$ always holds.

It should be noted that in this paper, DS is numerically equivalent to the sum of the elements of adjacency matrix as topological representations of graph connectivity. According to [18], under the same condition of the length of input samples and the number of graph vertices, the stronger the connectivity of the graph, the more uniform the VPV, and the larger the DS and the sum of the elements of the adjacency matrix. Therefore, both DS and the sum of the elements of the adjacency matrix can represent the strength of graph connectivity. Of course, other features reflecting graph connectivity, such as the eigenvalues of the Laplacian matrix [22] and the total number of graph edges [13], can also be used to characterize the strength of

graph connectivity. In this paper, DS is calculated as graph feature in all simulations. **Table 2** shows the coefficient values c_1d_1, c_2d_2 and DS values ϕ_1, ϕ_2 obtained from 10 times simulations when the observed signal are the constant with AGWN of variances $\sigma_1^2=10$ and $\sigma_2^2=1$, respectively, where $R=1$. The parameter settings are as follows: the length of the signal samples $N=1000$, and the number of graph vertices $N_0=20$. For simplification of expression, the generated graph with noise variance $\sigma_1^2=10$ is denoted as G_{σ_1}, and the generated graph with noise variance $\sigma_2^2=1$ is denoted as G_{σ_2}. The flag of order-preserving is indicated by '1', otherwise it is indicated by '0'.

Table 2. The coefficients and DS values under different noise variances

index / record	1	2	3	4	5	6	7	8	9	10
c_1d_1	3.076	2.518	2.773	3.038	3.205	3.675	3.522	2.873	3.445	2.805
c_2d_2	2.297	2.772	2.338	2.438	2.477	2.445	2.506	2.123	2.238	2.233
ϕ_1	250	282	254	222	240	188	236	262	202	250
ϕ_2	226	206	256	208	214	224	278	264	280	242
Order-preserving label	1	1	0	1	1	0	0	0	0	1

In **Table 2**, for the 2nd simulation, the coefficients c_1d_1 and c_2d_2 satisfy the order-preserving condition of Theorem 1, i.e., $c_1d_1 < c_2d_2$, then $\phi_1 > \phi_2$, which indicates that the connectivity of G_{σ_1} is greater than the connectivity of G_{σ_2}. However, for the 1st, 4th, 5th, and 10th simulation, although the connectivity of G_{σ_1} is greater than the connectivity of G_{σ_2}, the coefficients c_1d_1 and c_2d_2 do not satisfy the order-preserving condition in Theorem 1. From this, it can be seen that $c_1d_1 < c_2d_2$ is a sufficient but not necessary condition for realizing order-preserving between input majorization order and quantization majorization order. From another perspective, if order is not preserved between input majorization order and quantization majorization order, then $c_1d_1 < c_2d_2$ cannot hold, as seen in index 3rd, 6th, 7th, 8th, and 9th simulation trails.

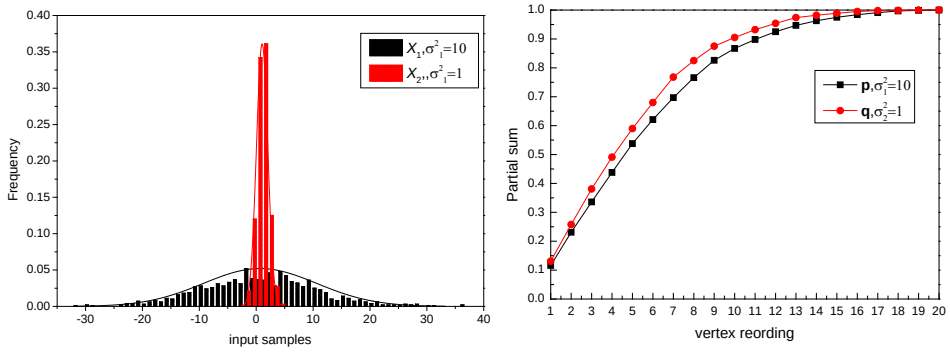

(a) PDF of the input samples (b)Partial sum of VPV

Fig. 1. PDF of the input samples and its partial sum of VPV.

Fig. 1 shows the the PDF of the input samples with AGWN of different variances for graph transformation and the corresponding partial sums of VPVs in an individual simulation trial.

As shown in **Fig. 1 (a)**, $f_{X_1}(x) \prec f_{X_2}(x)$ holds, indicating that X_1 is more uniform compared to X_2. Similarly, in **Fig. 1 (b)**, there is $\mathbf{p} \prec \mathbf{q}$, indicating that $\mathbf{p}$ is more uniform compared to $\mathbf{q}$. In this case, the input majorization order and the quantization majorization order is order preserving. Based on the above analysis, we attempt to use the OPR of the majorization order as a quantitative criterion to determine whether the connectivity of the graph approximately decreases monotonically as the variance of the AGWN decreases. Hence, the OPR of the majorization order is defined as:

$$\eta = \mathbf{I}(f_{X_1} \prec f_{X_2} \Rightarrow \mathbf{p} \prec \mathbf{q}) / N_e, \tag{12}$$

where N_e is the number of simulations, $\mathbf{I}(Z)$ is an indicator function that takes the value 1 when Z is true and 0 when Z is false. From this, we can calculate that the OPR in **Table 2** is 50%. Clearly, the higher the OPR, the better the monotonicity of the approximate decrease in graph connectivity as the variance of the Gaussian noise increases. Conversely, the lower the OPR, the worse the monotonicity.

In this paper, the input samples for the graph transformation are frequency band binary phase shift keying (BPSK) signals with AGWN unfortunately. It is difficult to obtain an analytical expression for the PDF of the input samples. However, the issue of order-preserving between input majorization order and quantization majorization order under different noise variances still exists. Moreover, it is also difficult to analysis analytically and we resort to simulation. If the BPSK signal is a deterministic signal, the PDF of the samples obtained by adding AGWN to the deterministic signal can be calculated by convolving the statistical histogram of the deterministic signal with the statistical histogram of the Gaussian distributed random variable. Since the BPSK signal is deterministic, the convolution result mainly depends on the distribution of the Gaussian distributed random variable. According to the property of convolution, if the variance of the Gaussian distributed random variable is larger, the PDF of the Gaussian distributed random variable becomes more uniform, and the convolution becomes more uniform, and vice versa. Furthermore, we use some simulations to verify this conclusion.

Fig. 2 shows the PDFs of input samples of BPSK signals with AGWN of different variances, and their non-increasing rearrangement of VPVs. The parameters are set as follows, the signal amplitude $A = 4$, carrier frequency $f_0 = 20.76\text{MHz}$, the symbol width are 640ns, the sampling interval $\Delta t = 100\text{us}$, the sample length $N = 1000$, the initial phase $\theta = \pi/4$, and the number of graph vertices $N_0 = 20$. It can be seen that the input samples with larger variance have a more uniform distribution, and the VPV with larger variance is also more uniform, too, which verifying the above conclusion and shows that the order is preserved in this case.

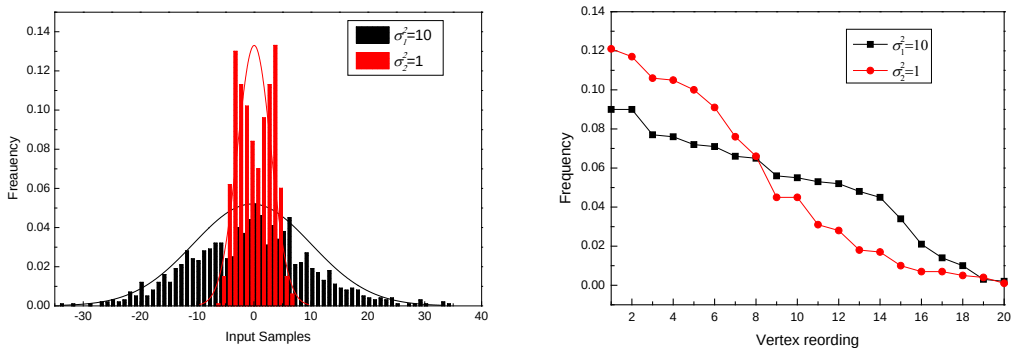

(a) PDFs of input samples (b) the non-increasing rearrangements of VPVs

Fig. 2. PDFs of input samples and their non-increasing rearrangements of VPVs.

Table 3 shows the DS value of ϕ_1 and ϕ_2, and order-preservation labels when the input samples are BPSK signals added with AGWN, where the variances are $\sigma_1 = 10$ and $\sigma_2 = 1$, respectively. It can be observed that the OPR is 30% when transforming the input samples in time domain to graph directly. Therefore, it is necessary to preprocess and modify the input samples before graph transformation in order to increase the OPR and enhance order-preserving ability of the input majorization order for improving the graph-based SNR estimation.

Table 3. DS values under different noise variances

index / record	1	2	3	4	5	6	7	8	9	10
ϕ_1	196	248	228	276	234	240	218	216	254	228
ϕ_2	238	252	226	230	266	276	264	238	250	238
Order-preserving label	0	0	1	1	0	0	0	0	1	0

3.3 Graph-based SNR estimation using SBS

The proposed graph-based SNR estimation algorithm using SBS consists of two main stages: expression fitting and SNR estimation. The detailed description of the proposed algorithm is provided below:

Stage 1: Expression fitting.

Input: Observed signal $x(n)$, signal length N, number of vertices N_0, length of segmented samples in the overlapping segmentation step l, length of overlapping samples h, number of segments m, length of block samples within each segment a.

Output: SNR estimation expression $\beta = f(\alpha)$.

Process:

a) Segment the observed signal $x(n)$ with overlapping to obtain $\rho_1(\theta), \rho_2(\theta), ..., \rho_m(\theta), 1 \le \theta \le l$, where $N = (l\text{-}h) \times (m\text{-}1) + l$.

b) Calculate the spectrum of $\rho_1(\theta), \rho_2(\theta), ..., \rho_m(\theta), 1 \le \theta \le l$ and get the real parts of them, denoted as $s_1(\theta), s_2(\theta), ..., s_m(\theta)$.

c) Block and sum the samples of $s_i(\theta), 1 \le i \le m$ with length of samples a, and obtain a SBS sequence as $\Psi_i(\tau), 1 \le i \le m, 1 \le \tau \le \left\lfloor l/a \right\rfloor$.

d) Convert $\Psi_i(\tau), 1 \le i \le m$ into graphs $G_1(E_1, V_1), G_2(E_2, V_2), ..., G_m(E_m, V_m)$ with N_0 vertices.

e) Calculate the average DS of the graph $G_1(E_1, V_1), G_2(E_2, V_2), ..., G_m(E_m, V_m)$.

f) Correlate the average DS α obtained for each SNR with the corresponding SNR and fit the expression $\beta = f(\alpha)$.

Stage 2: SNR estimation.

Input: Test signal $x_1(n)$.

Output: Estimation of SNR $\hat{\beta}$.

Process:

a) Calculate the average DS α_1 of the test signal $x_1(n)$ using stages (a) ~ (e) in Step 1.

b) Substitute α_1 into the fitting expression $\beta = f(\alpha)$ to obtain the estimation of SNR $\hat{\beta}$.

Intuitively, the main indicators for evaluating the robustness of SNR estimation algorithms are the monotonicity and rate of change of the DS with respect to SNR. Firstly, it is necessary to ensure the monotonicity of the fitting curve of SNR estimation. If the relationship between DS and SNR is not monotonical, it will result in estimation ambiguity between the DS and SNR. Secondly, when satisfying the monotonicity condition, further observation of the rate of change of the fitting curve is also important. If the rate of change of the curve is faster, it indicates that there is a significant difference in DS corresponding to adjacent SNRs, which is beneficial for improving estimation performance. Furthermore, if the monotonicity of the curve and the rate of change are not significantly different, the variance of DS corresponding to the same SNR is another important factor effecting SNR estimation performance. Intuitively, larger variance of DS results in larger estimation error. Therefore, the monotonicity, the rate of change, and the variance of DS with respect to SNR are three important indicators for evaluating performance of estimation algorithm. A monotonic curve with a faster rate of change and a smaller variance of DS generally results in smaller estimation errors. Inspired by [23], we define the deflection coefficient of DS as indicators for evaluating the differences in connectivity of generated graph under adjacent SNRs, as follows:

$$DIS_{ij} = \frac{\mathrm{E}[\beta]_i - \mathrm{E}[\beta]_j}{var_i}, i, j = 1,.., N_s, \tag{13}$$

where $\mathrm{E}[\beta]_i$ is the average DS under idB, $\mathrm{E}[\beta]_j$ is the average DS of under jdB, N_s is number of SNR investigated in simulations, and $var_i = [\mathrm{var}[\beta]_i + \mathrm{var}[\beta]_j]/2$ is the average of the variance. Intuitively, the higher the OPR, the better the monotonicity of the fitting curve, and the larger the deflection coefficient, accordingly, the more favorable the accuracy of the graph-domain SNR estimation. Here, we verify the relationship between the OPR and the deflection coefficient by simulation. At the same time, in order to solve the two problems mentioned before, namely, the low OPR of directly using the real part of the observed signal in the time-domain for graph transformation and the fact that the algorithm in [11] is only applicable to baseband signals, we attempt to utilize the SBS as the input fed to graph transform. Specifically speaking, the observed signal is segmented by overlapping, and then the real part of the spectrum of each segment is blocked and summed to construct a graph by which the average DS is calculated.

Table 4 shows the OPR and the deflection coefficient of the proposed algorithm and the existing algorithm in [11] under different SNRs with 1000 trails. In each simulation, 20 sets of training samples are obtained, and the average DS from these 20 sets are calculated, following the same conditions as in **Fig. 2**. It can be observed that under baseband conditions, at lower SNRs, the OPR and deflection coefficient of the proposed algorithm are significantly higher than the algorithm in [11]. At higher SNRs, the OPR are the same for both two algorithms, but the deflection coefficient of the proposed algorithm is much larger than that of the algorithm in [11]. Under frequency band conditions, both the OPR and deflection coefficient of the proposed algorithm are significantly higher than those of the algorithm in [11]. **Fig. 3** shows the deflection coefficient of the proposed algorithm and the existing algorithm in [11] for adjacent SNRs calculated from 20 sets of training samples. It can be observed that for both frequency band and baseband signals, the deflection coefficient obtained by the proposed algorithm is significantly larger than that of the algorithm in [11].

Table 4. Comparison of OPR and deflection coefficient between the proposed algorithm and the algorithm in [11]

index / record	baseband SNR=0,5dB	baseband SNR=5，20dB	frequency band SNR=0,5dB	frequency band SNR=5，20dB
OPR/ deflection coefficient of the proposed algorithm	100%/5.12	100%/24.25	100%/6.42	100%/24.06
OPR/ deflection coefficient in [11]	54%/1.58	100%/20.8	10%/-0.87	0/3.69

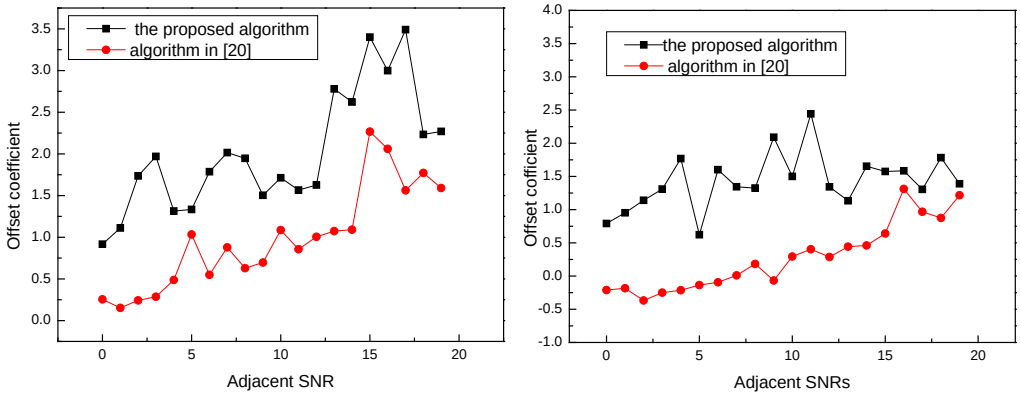

(a)baseband signal (b)frequency band signal

Fig. 3. Comparison of deflection coefficients between the proposed algorithm and the algorithm in [11].

3.4 Algorithm complexity analysis

Here, we analyze the computational complexity of the main steps in the proposed algorithm, and compare with that of the algorithm in [11].

The complexity of the proposed algorithm involves the following steps: 1) The computational complexity of calculating the real part of the spectrum for each segment after overlapping segmentation is approximately $O(l\log_2^l)$. 2) In the grouping and summation step, the number of addition operations within each segment is $(a-1)a_0$, resulting in a computational complexity of approximately $O(l)$, where $a_0 = \left\lceil l/a \right\rceil$. 3) For the graph transformation step, the input sample size is a_0. After obtaining the maximum and minimum values of the graph input during the normalization process, an addition and a multiplication operation are performed. The quantization requires a_0 comparisons, and $a_0 - 1$ comparisons are needed to compare adjacent vertices and construct the edges of the graph. Therefore, the computational complexity is approximately $O(a_0)$. 4) Calculating the DS requires a_0^2 addition operations, resulting in a computational complexity of $O(a_0^2)$. Overall, the computational complexity of processing one segment sample is approximately $O(l\log_2^l + l + a_0 + a_0^2)$. Therefore, the computational complexity of performing the above operations on one observed signal is approximately $O(ml\log_2^l + ml + ma_0 + ma_0^2)$.

The main steps and their computational complexity analysis of the algorithm in [11] is as follows: 1) After overlapping segmentation, the graph transformation is performed for each segment. The input sample length for graph transformation is l. The normalization, quantization, and graph mapping steps are the same as in the proposed algorithm, resulting in a computational complexity of $O(l)$. 2) Calculating the sum of the adjacency matrix of the

graph require l^2 addition operations, resulting in a computational complexity of $O(l^2)$. Overall, the computational complexity of processing one segment sample is approximately $O(l+l^2)$. Therefore, the computational complexity of performing the above operations on one observed signal is approximately $O(ml+ml^2)$.

Considering that a is generally selected to be 5~10, we have $a_0 << l$. Therefore, the computational complexity of the algorithm in [11] is significantly greater than that of the proposed algorithm.

Remarks: For a given original power spectrum (OPS) of the observed signal contained by AWGN, the connectivity of the graph transformed from OPS is approximated to that generated from SBS [17]. This is the main reason that we utilized the block processing.

4. Performance simulation

This section will accomplish the following tasks: 1) Curve fitting method of the proposed algorithm and its evaluation under different noise backgrounds and channel conditions; 2) Analysis of the impacts of different parameters on the performance of the graph-based SNR estimation algorithm proposed in this paper; 3) Comparison of the performance of the proposed algorithm in this paper, the algorithm in reference [11], and the M2M4-based SNR estimation algorithm in [7] using the normalized root mean square error (NRMSE) and computational complexity as the metric. NRMSE is defined as

$$NMRSE(\hat{\Gamma}) = \frac{1}{\Gamma_i}\sqrt{\frac{1}{\psi}\sum_{i=1}^{\psi}(\hat{\Gamma}_i - \Gamma_i)^2}\ , \tag{14}$$

where ψ is the times of simulations, $\hat{\Gamma}_i$ is obtained via $\hat{\Gamma}_i = 10^{\hat{\beta}_i/10}$ in the ith simulation, where $\hat{\beta}_i$ is the estimated value of SNR, and Γ_i is obtained via $\Gamma_i = 10^{\beta/10}$, where β is the true value of SNR.

Unless otherwise specified, the observed signal is a BPSK signal including AGWN with range of the SNR varying from 0 to 20dB. The signal parameters are consistent with **Fig. 2**, and the parameters involved in the signal transformation processes are shown in **Table 5**.

Table 5. Parameters involved in the signal transformation process

Signal transformation process	Parameter name	Value
Overlapping segment	length of segmented samples l	200,100,50
	length of overlapping samples h	0,10,50
	number of segments m	20
SBS	length of block samples within each segment a	5,10,20
Graph transformation	number of vertices N_0	40

4.1 Curve fit performance evaluation based on SBS

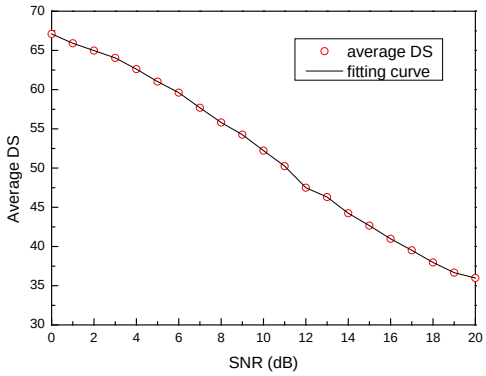

Fig. 4. Relationship between the average DS of and SNR, along with the fitting curve.

Fig. 4 represents relationship between the average DS of and SNR, along with the Fitting Curve, when the length of segmented samples $l=200$, the length of overlapping samples $h=10$, and the length of block samples within each segment $a=5$. The average DS decrease monotonically as the SNR increases during the fitting process. By applying the trust-region algorithm [24] for nonlinear fitting based on the obtained average SD under each SNR condition, an expression for estimating SNR is obtained by

$$\beta=f(\alpha)=-0.0001533\times\exp(0.1573\times\alpha)+83.34\times\exp(-0.03998\times\alpha) \quad (15)$$

Next, we further analyze the mapping relationship between the average DS and SNR under different types of noise distributions and channel conditions.

4.1.1 Different types of noise distributions

Fig. 5 presents the average DS versus SNR under different noise distributions when the length of segmented samples $l=200$, the length of overlapping samples $h=10$, and the length of block samples within each segment $a=5$. It can be seen that not only Gaussian noise but also other non-Gaussian noise distributions such as the exponential, uniform, Chi-square, and Laplacian noises, all exhibit a monotonically decreasing trend in the average DS as the SNR increases, which indicates that the proposed algorithm is effective for various types of noise distributions considered in the wireless communications.

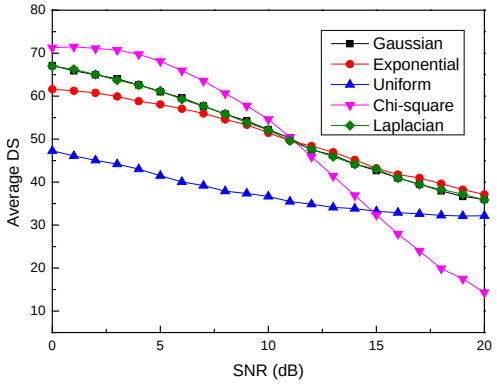

Fig. 5. The average DS versus SNR under different noise distributions.

4.1.2 Different types of channels

Fig. 6 presents the average DS versus SNR under different channels when the length of segmented samples $l = 200$, the length of overlapping samples $h = 10$, and the length of block samples within each segment $a = 5$. According to the definition in (2), channels can be categorized into four types: Channel I: $c(n) = \delta(n-1) + \delta(n-2) + \delta(n-3)$, Channel II: $c(n) = \delta(n-1) + 0.2\delta(n-2) + 0.5\delta(n-3)$. Channel III: a frequency-flat Rayleigh fading channel with a maximum Doppler shift of 130Hz, featuring only one path with no delay, and a single path gain of -6dB. Channel IV: a frequency-selective Rayleigh fading channel with a maximum Doppler shift of 130Hz, having four paths with delays of $0, 5\Delta t, 10\Delta t, 15\Delta t$ respectively, and multi-path gains of 0dB, -3dB, -6dB, and -9dB respectively. Clearly, in various channels, as SNR increases, the estimated SNR values generally show a decline trend. However, for Channel III and Channel IV, when the SNR is high, there is a small local fluctuation in the estimated SNR values. Furthermore, the rates of decrease are relatively similar among the above mention five cases. This indicates that the proposed algorithm remains effective under the five kinds of channels provided in the simulations when SNR is less than 10dB.

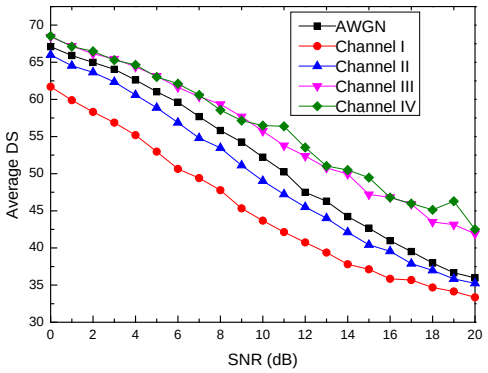

Fig. 6. The average DS versus SNR under different channels.

4.2 Evaluation performance

4.2.1 Different lengths of segmented samples

Fig. 7 presents the average DS versus SNR under different lengths of segmented samples when the length of segmented samples $l = 200,100,50$, the length of overlapping samples $h = 10$, and the length of block samples within each segment $a = 5$. As the length of segmented samples decreases, the rate of change in average DS decreases. This phenomenon is attributed to the decrease in the number of samples used for graph transformation due to the reduction in length of segmented samples, resulting in smaller differences in graph connectivity under different SNR. **Fig. 8** presents the influence of length of segmented samples on the estimation performance. In the entire range of SNR, as the length of segment samples decreases, the NRMSE increases. Therefore, increasing the segment length can enhance the distinguishability of graph connectivity under different SNR, thereby improving the SNR estimation performance. However, it should be noted that this causes higher computational complexity. Hence, when taking graph connectivity distinguishability and computational complexity into consideration, it is crucial to carefully select an appropriate length of segmented samples.

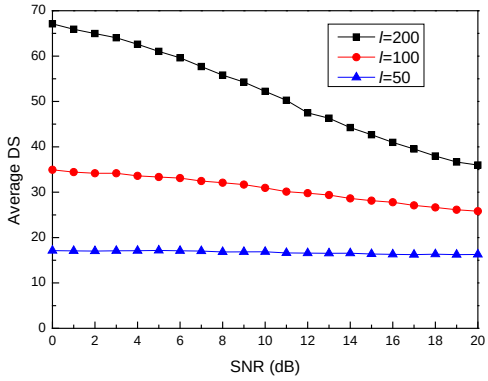

Fig. 7. The average DS versus SNR under different length of segmented samples.

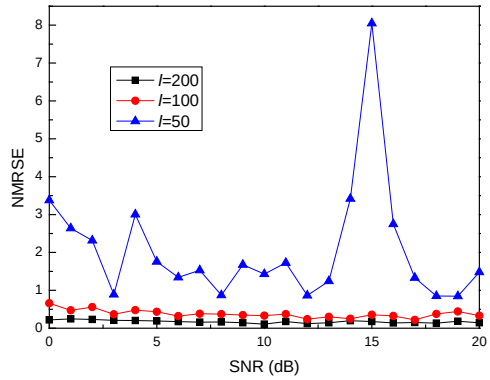

Fig. 8. The influence of length of segmented sample on the estimation performance.

4.2.2 Different lengths of overlapping samples

Fig. 9 presents the average DS versus SNR under different lengths of overlapping samples, when the length of segmented samples $l = 200$, the length of overlapping samples $h = 0{,}10{,}50$, and the length of block samples within each segment $a = 5$. The rate of change in average DS remains relatively consistent. Additionally, the range of the average DS also remains similar. This indicates that the variation in length of overlapping sample has similar impact on the graph connectivity. **Fig. 10** presents influence of the number of overlapping samples on the estimation performance. It can be observed that, at the same SNR, the variation in the number of overlapping samples does not significantly affect the NRMSE. The purpose of applying overlapping processing to the segmented samples is to generate more segments where the input sample size is relatively small and increases the number of input sample of graph transformation, thereby improving the accuracy and stability of the SNR estimation curve fitting.

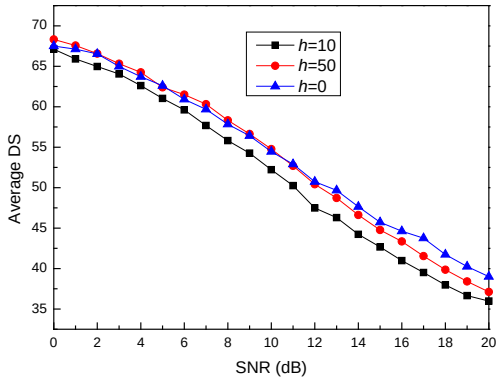

Fig. 9. The average DS versus SNR under different lengths of overlapping samples.

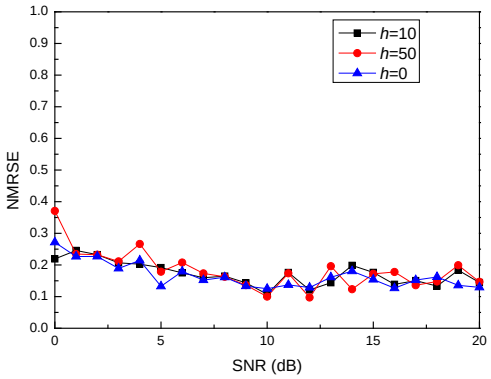

Fig. 10. Influence of the length of overlapping samples on the estimation performance.

4.2.3 Different lengths of block samples within each segment

Fig. 11 presents the average DS versus SNR under different lengths of block samples within each segment when the length of segmented samples $l = 200$, the length of overlapping samples $h = 10$, and the length of block samples within each segment $a = 5,10,20$. As the length of block samples increases, the rate of change in average DS decreases. This is because an increase in the length of block samples leads to a reduction in the number of input samples of graph transformation, resulting in fewer changes in graph connectivity with varying SNR. Therefore, reducing the length of block samples appropriately can enhance the distinguishability of graph connectivity under different SNR. **Fig. 12** presents influence of lengths of block samples within each segment on the estimation performance. As the length of block samples increases, the NRMSE also increases. Therefore, reducing the length of block samples is beneficial for improving the SNR estimation performance. However, it should be noted that this will bring increasing computational complexity and a loss of statistical significance. Generally, it is recommended to have a group size of at least 40 samples after grouping. In this case, $a = 5$ is chosen.

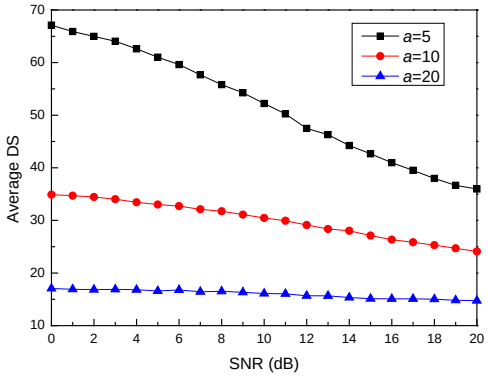

Fig. 11. The average DS versus SNR under different lengths of block samples within each segment.

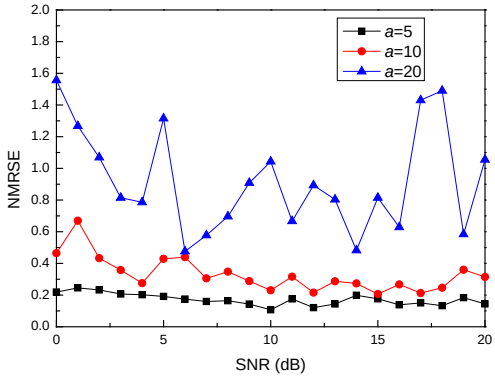

Fig. 12. Influence of length of block samples within each segment on the estimation performance.

4.2.4 Different step sizes for graph transformation

Fig. 13 presents the average DS versus SNR under different graph mapping step sizes. When using multi-step sizes for graph edge construction, the average DS exhibit a monotonically decreasing trend as the SNR increases. Furthermore, their rate of change is significantly faster compared to the case of a single-step size. **Fig. 14** presents boxplot of DS under different graph mapping step sizes, while **Fig. 15** shows comparison of deflection coefficients under different graph mapping step sizes. The DS value and its variance of the graph obtained through a single-step size graph mapping are generally smaller than those of the graph obtained through multi-step size graph mapping. Therefore, we choose a single step in the graph mapping process. Additionally, the deflection coefficients of the single-step size transformation graphs are generally larger than those of the multi-step size transformation graphs. **Fig. 16** presents impact of graph mapping step size on the estimation performance. When the SNR is greater than 7dB, the estimation performance of the single-step size outperforms that of the multi-step size, confirming the previously mentioned conclusion.

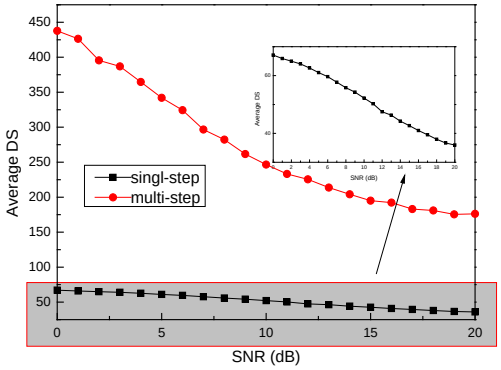

Fig. 13. The average DS versus SNR under different graph mapping step sizes.

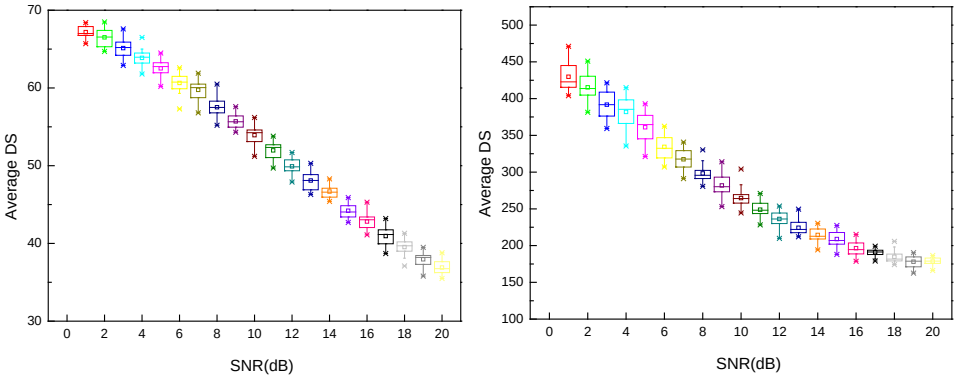

(a)single-step (b)multi-step

Fig. 14. Boxplot of DS under different graph mapping step sizes.

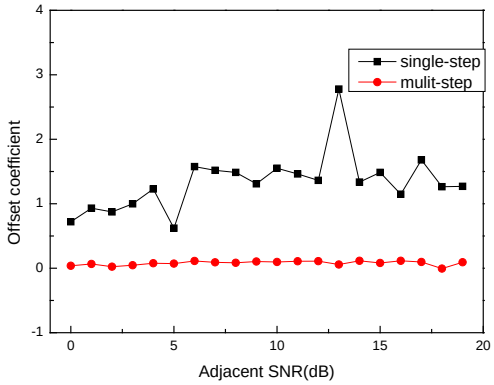

Fig. 15. Comparisons of deflection coefficients under different graph mapping step sizes.

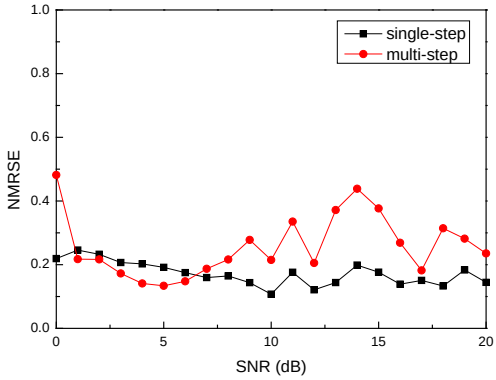

Fig. 16. Impact of graph-mapping step size on the estimation performance.

4.3 Performance comparison with existing algorithms

4.3.1 Comparisons of performance on estimation

Fig. 17 presents performance comparisons of the proposed algorithm (denoted as GSBF), graph-based SNR estimation algorithm based on the time-domain signal [11] (denoted as GSET), M2M4 [7] and SVD [8] under condition of AWGN. The simulation conditions are provided in **Table 5**, and BPSK signal parameters are the same as set in **Fig. 2**. Note that, since GSET fails to exhibit a monotonic relationship between the graph connectivity and the SNR for a frequency band signal, GSET was modified by performing segmented fitting to make comprehensive comparisons. Specifically, the fitting was done separately for SNRs below 11dB and those above 11dB, resulting in segmented fitting curves for SNR estimations. As can be seen from the figure, for frequency band signals, GSBF outperforms GSET and M2M4, especially, when the SNR ranges from 3dB to 15dB. For baseband signals, GSBF performs better than M2M4 and is essentially equivalent to GSET. Additionally, regardless of a frequency band or base band signal, when the SNR varies from 13dB to 20dB, GSBF performs noticeably better than SVD. When SNR is low, SVD has the most advantageous performance of all the mentioned algorithms, but it has a high computational complexity, which is expressed in **Table 6**.

Fig. 18 compares the performances of the proposed algorithm with three others under multipath channels. In this case, Channel II: $c(n) = \delta(n-1) + 0.2\delta(n-2) + 0.5\delta(n-3)$. Intuitively, for frequency band signals, GSBF performs better than GSET when the SNR ranges from 3dB to 9dB. Moreover, when the SNR ranges from 1dB to 20dB, GSBF performs better than M2M4 and SVD. For baseband signals, GSBF outperforms M2M4 and SVD, but is slightly inferior to GSET. It's worth mentioning that compared to the other three algorithms, the performance curve of our algorithm does not change much.

Fig. 19 shows the performances of the proposed algorithm versus three others under fading channels, i.e., Channel III. For frequency band signals, overall, GSBF performs better than M2M4 and GSET, but it is inferior to SVD when SNR is low. For baseband signals, GSBF is significantly better than M2M4, and at high SNR, it performs better than SVD but slightly worse than GSET.

Fig. 20 illustrates the comparative performance of GSBF, SVD and GSET under Channel IV. It should be noted that by simulations we found that under a frequency-selective Rayleigh channel, GSET fails for SNR estimation of frequency band signals, and M2M4 may yield negative SNR estimate for both frequency band and base band signals. Due to the failure of

the two algorithms under this channel, the performance of GSET and M2M4 were not depicted in **Fig. 20 (a)**, and M2M4 was not considered in **Fig. 20 (b)**. The figures show that our algorithm outperforms SVD under low SNR for frequency band signals and significantly surpasses GSET for baseband signals. Overall, the proposed algorithm (GSBF) and SVD are less affected by the channel. From the perspective of computational complexity, our method has an advantage over SVD requiring matrix decomposition with computational complexity order of $O(N^3)$, where N is the matrix dimension.

In summary, the proposed algorithm outperforms M2M4, excels GSET for frequency band signals. and outperforms SVD under multipath channels. Additionally,the performance curve of our algorithm is the most stable as well.

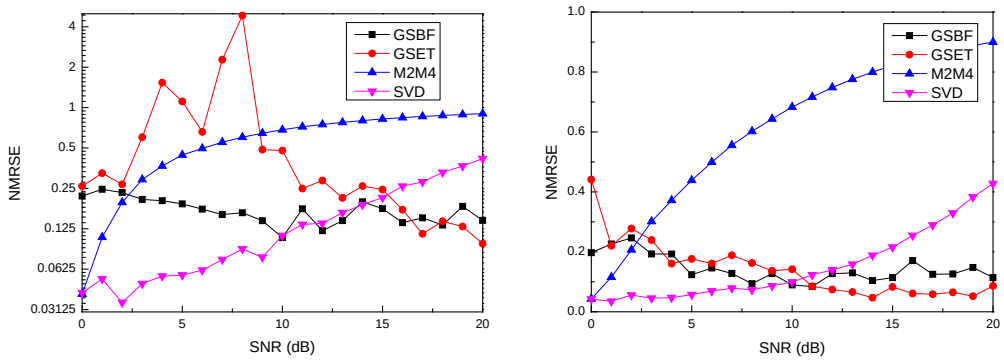

(a)frequency band signal (b)baseband signal

Fig. 17. Performance comparisons of the proposed algorithm and other algorithms under AWGN.

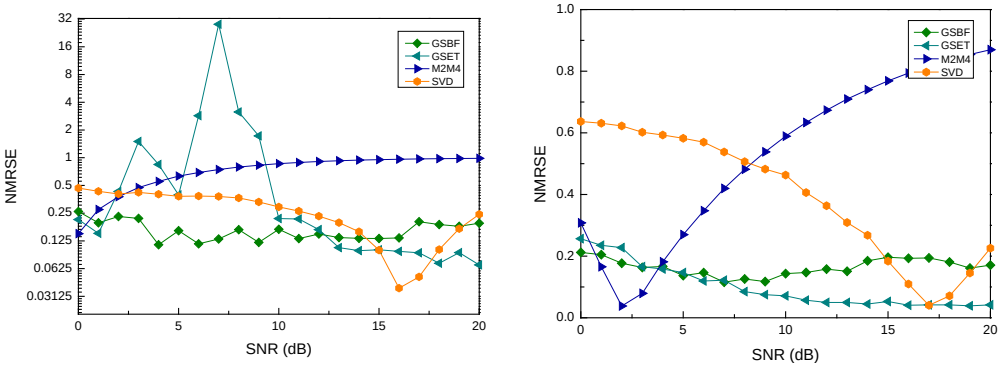

(a)frequency band signal (b)baseband signal

Fig. 18. Performance comparisons of the proposed algorithm and other algorithms under multipath channels (Channel II).

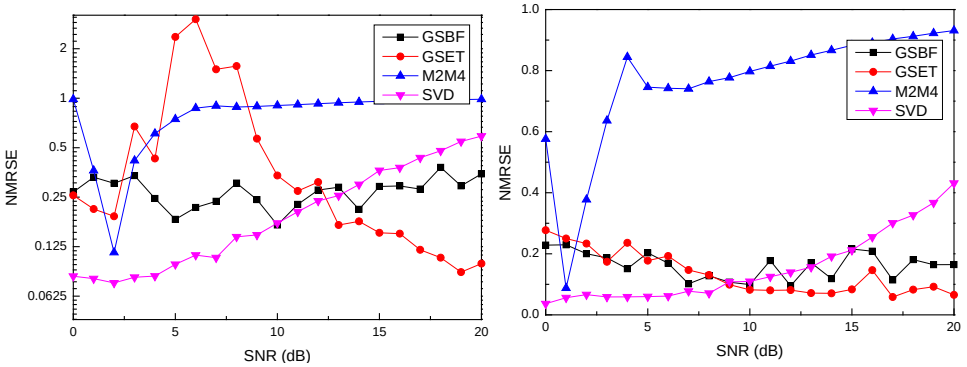

(a)frequency band signal (b)baseband signal

Fig. 19. Performance comparisons of the proposed algorithm and other algorithms under fading channels (Channel III).

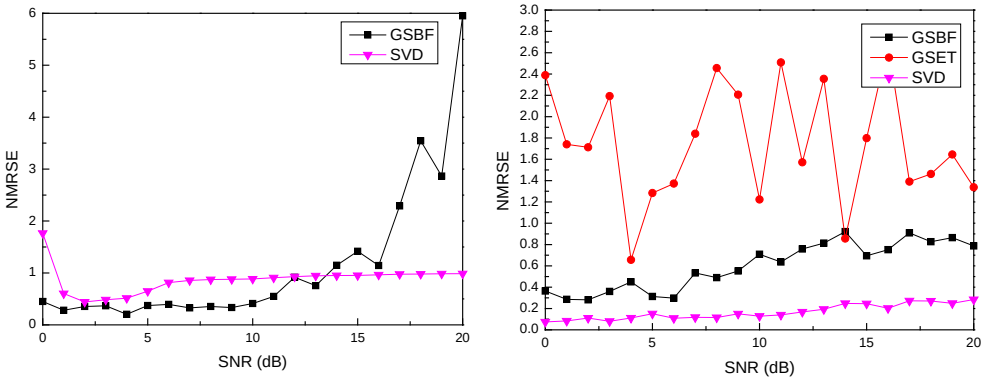

(a)frequency band signal (b)base band signal

Fig. 20. Performance comparisons of the proposed algorithm and other algorithms under Channel IV.

4.3.2 Comparison of computational complexity

Table 6 presents the computational complexity orders and the average running time required to complete one estimation for the four algorithms. The training time is obtained by performing 20 simulations when SNR ranges from 1dB to 20dB, and the testing time is the average of 1000 simulations. The simulation conditions are the same as in **Fig. 17 (a)**, where $N \approx ml$. The hardware platform used in the simulation is Intel(R) Core(TM) i7-8550U CPU (1.80GHz), and the software platform is MATLAB R2021a. Except for the M2M4 and SVD, which does not require training, the total computation time of GSBF is approximately 50% of the total computation time of GSET under the same conditions. In conclusion, considering both estimation performance and computational complexity, GSBF has the best overall performance.

Table 6. Comparison of computational complexity for different algorithms.

Algorithm	Computational complexity order	Training time(ms)	Testing time(ms)	Total time(ms)
GSBF	$O(ml\log_2^l + ml + ma_0 + ma_0^2)$	1752	3.09	1755.09
GSET	$O(lm + l^2 m)$	3824	8.55	3832.55
M2M4	$O(N)$	-	11.02	11.02
SVD	$O(N^3)$	-	1831.8	1831.8

5. Conclusion

An improved graph-based SNR estimation algorithm using SBS is proposed in this article. The main contribution of this paper lies in introducing OPR and deflection coefficient as indicators to guide the selection of inputs for graph-based SNR estimation, and analyzing the order-preserving about majorization relationships between the input and quantization samples in the graph transform. Simulation results demonstrate that the proposed method effectively establishes a functional mapping from the average DS to SNR values. The influence of various parameters, such as length of segmented samples, length of overlapping samples, and length of block samples within each segment on the estimation performance is analyzed, and the simulation results indicate that the variation of length of overlapping samples has no impact on performance, whereas both excessively large length of block samples within each segment and too small length of segmented samples will affect the estimation performance. Additionally, when the signal type varies and the channel experiences constant multipath or fading, this algorithm remains effective. Compared with the existing graph-based SNR estimation method, the proposed algorithm is applicable to both frequency band and baseband signals, exhibiting better estimation performance with lower computational complexity under low SNRs. However, there still exists several limitations in the article. It can be briefly summarized as follows: 1) the proposed algorithm only utilizes simple graph transformations without considering additional graph information such as self-loops or directionality, which capture more topological information about the signals; 2) the function between the DS and the SNR didn't consider the utilization of the machine learning network. In future research, we will investigate other techniques like Graph Convolutional Neural Network to develop novel graph-based SNR estimation methods.

Acknowledgements

This study was financially supported by the Natural Science Foundation of the Jiangsu Higher Education Institutions of China (Project No. 20KJA510008), and Training Program of Innovation and Entrepreneurship for Undergraduates (Project No. 202313573083Y).

References

[1] D.R. Pauluzzi and N.C. Beaulieu, "A comparison of SNR estimation techniques for the AWGN channel," *IEEE Transactions on Communications*, vol.48, no.10, pp.1681-1691, 2000. Article(CrossRef Link)

[2] R. Tandra and A. Sahai, "SNR Walls for Signal Detection," *IEEE Journal of selected topics in Signal Processing*, vol.2, no.1, pp.4-17, 2008. Article(CrossRef Link)

[3] T. L. Marzetta, "Noncooperative Cellular Wireless with Unlimited Numbers of Base Station Antennas," *IEEE transactions on wireless communications*, vol.9, no.11, pp.3590-3600, 2010. Article(CrossRef Link)

[4] X. Yi and C. Zhong, "Deep Learning for Joint Channel Estimation and Signal Detection in OFDM Systems," *IEEE Communications Letters*, vol.24, no.12, pp.2780-2784, 2020. Article(CrossRef Link)

[5] H. S. Liao, L. Gan, and P. Wei, "A blind SNR estimation method for radar signals," in *Proc. of 2009 IET International Radar Conference*, pp.1-4, 2009. Article(CrossRef Link)

[6] N. Wu, H. Wang, and J.-M. Kuang, "Maximum likelihood signal-to-noise ratio estimation for coded linearly modulated signals," *IET Communications*, vol.4, no.3, pp.265-271, 2010. Article(CrossRef Link)

[7] G. Romano, "On Asymptotic Efficiency of the *M2M4* Signal-to-Noise Estimator for Deterministic Complex Sinusoids," *Sensors*, vol.21, no.15, 2021. Article(CrossRef Link)

[8] X. Zhang and Z. Dong, "Research on SVD SNR Estimation Algorithm," in *Proc. of 2022 12th International Conference on Information Technology in Medicine and Education (ITME)*, pp.569-574, 2022. Article(CrossRef Link)

[9] S. Barbarossa and S. Sardellitti, "Topological Signal Processing: Making Sense of Data Building on Multiway Relations," *IEEE Signal Processing Magazine*, vol.37, no.6, pp.174-183, 2020. Article(CrossRef Link)

[10] H. Li, D. Wang, X. Zhang, and G. Gao, "Frame-Level Signal-to-Noise Ratio Estimation Using Deep Learning," in *Proc. of Interspeech 2020*, pp.4626-4630, 2020. Article(CrossRef Link)

[11] K. Yan, H.-C. Wu, and X. Huang, "Blind SINR Estimation Based on Graph Sparsity," in *Proc. of GLOBECOM 2020 - 2020 IEEE Global Communications Conference*, pp.1-7, 2020. Article(CrossRef Link)

[12] K. Yan, H.-C. Wu, H. Xiao, and X. Zhang, "Novel Robust Band-Limited Signal Detection Approach Using Graphs," *IEEE Communications Letters*, vol.21, no.1, pp.20-23, 2017. Article(CrossRef Link)

[13] K. Yan, H.-C. Wu, C. Busch, and X. Zhang, "Graph representation of random signal and its application for sparse signal detection," *Digital Signal Processing*, vol.96, 2020. Article(CrossRef Link)

[14] Y. A. Eldemerdash, O. A. Dobre, O. Üreten, and T. Yensen, "A Robust Modulation Classification Method for PSK Signals Using Random Graphs," *IEEE Transactions on Instrumentation and Measurement*, vol.68, no.2, pp.642-644, 2019. Article(CrossRef Link)

[15] L. Pu, H.-C. Wu, K. Yan, Z. Gao, X. Wang, and W. Xiang, "Novel Three-Hierarchy Multiple-Tag-Recognition Technique for Next Generation RFID Systems," *IEEE Transactions on Wireless Communications*, vol.19, no.2, pp.1237-1249, 2020. Article(CrossRef Link)

[16] X. Yan, G. Liu, H.-C. Wu, G. Zhang, Q. Wang, and Y. Wu, "Robust Modulation Classification Over α-Stable Noise Using Graph-Based Fractional Lower-Order Cyclic Spectrum Analysis," *IEEE Transactions on Vehicular Technology*, vol.69, no.3, pp.2836-2849, 2020. Article(CrossRef Link)

[17] G. Hu, Z. Chen, P. Zhao, and L. Yang, "Graph-based confidence verification for BPSK signal analysis under low SNRs," *Signal Processing*, vol.206, 2023. Article(CrossRef Link)

[18] L. Yang, G. Hu, X. Xu, and P. Zhao, "Modulation Recognition of BPSK/QPSK Signals based on Features in the Graph Domain," *KSII Transactions on Internet and Information Systems*, vol.16, no.11, pp.3761-3779, 2022. Article(CrossRef Link)

[19] R. J. Hickey, "Continuous majorisation and randomness," *Journal of Applied Probability*, vol.21, no.4, pp.924-929, 1984. Article(CrossRef Link)
[20] B. Widrow, I. Kollar, and M.-C. Liu, "Statistical theory of quantization," *IEEE Transactions on Instrumentation and Measurement*, vol.45, no.2, pp.353-361, 1996. Article(CrossRef Link)
[21] G. Marsaglia and W. W. Tsang, "A Fast, Easily Implemented Method for Sampling from Decreasing or Symmetric Unimodal Density Functions," *SIAM Journal on Scientific and Statistical Computing*, vol.5, no.2, pp.349-359, 1984. Article(CrossRef Link)
[22] N. M. M. de Abreu, "Old and new results on algebraic connectivity of graphs," *Linear Algebra and its Applications*, vol.423, no.1, pp.53-73, 2007. Article(CrossRef Link)
[23] S. M. Kay, Fundamentals of statistical signal processing: estimation theory, Prentice-Hall, Inc., 1993. Article(CrossRef Link)
[24] J. Nocedal, S. J. Wright, Numerical Optimization, Springer Series in Operations Research and Financial Engineering, Springer, 1999. Article(CrossRef Link)

Li Yang received the M.S. degree in signal and information processing from Yangzhou University, China, in 2008. Currently, she is a senior experimentalist at College of Electronic and Information Engineering, Jinling Institute of Technology. Her main research interest includes graph-domain signal processing.

Haoyu Wei is a third-year student in College of Electronic and Information Engineering at Jinling Institute of Technology. His main research interest lies in the field of digital signal processing.

Guobing Hu received the M.S. and Ph.D. degrees in electronic and information engineering from Nanjing University of Aeronautics and Astronautics, China, in 2006 and 2011, respectively. Currently, he is a Professor in the Department of Electronics and Information Engineering, Jinling Institute of Technology, and is a visiting scholar at Southeast University. His main research interests are radar signal processing and digital signal processing, with a particular focus on non-cooperative communications, cognitive radio systems, and multiple-input multiple-output antenna systems.

Wenqing Zhu is a graduate student in College of Electronic and Information Engineering, Artificial Intelligence at Nanjing Forestry University. His main research interest lies in the field of graph signal processing.